PNAS RESEARCH ARTICLE | MICROBIOLOGY

Unraveling clonal CD8 T cell expansion and identification of essential factors in γ-herpesvirus-induced lymphomagenesis

Meijiao Gong[a,1], Françoise Myster[a,1], Abdulkader Azouz[b,c], Guillem Sanchez Sanchez[b,c,d,e], Shifang Li[a], Benoit Charloteaux[f], Bin Yang[a], Jenna Nichols[g], Lucas Lefevre[h], Justine Javaux[a], Sylvain Leemans[a], Olivier Nivelles[a], Willem van Campe[i], Stefan Roels[i], Laurent Mostin[i], Thierry van den Berg[i], Andrew J. Davison[g], Laurent Gillet[a], Timothy Connelley[h], David Vermijlen[b,c,d,e], Stanislas Goriely[b,c], Alain Vanderplasschen[a,e], and Benjamin G. Dewals[a,e,2]

Affiliations are included on p. 11.

Edited by David Knipe, Harvard Medical School, Boston, MA; received March 4, 2024; accepted July 1, 2024

Alcelaphine gammaherpesvirus 1 (AlHV-1) asymptomatically persists in its natural host, the wildebeest. However, cross-species transmission to cattle results in the induction of an acute and lethal peripheral T cell lymphoma-like disease (PTCL), named malignant catarrhal fever (MCF). Our previous findings demonstrated an essential role for viral genome maintenance in infected CD8$^+$ T lymphocytes but the exact mechanism(s) leading to lymphoproliferation and MCF remained unknown. To decipher how AlHV-1 dysregulates T lymphocytes, we first examined the global phenotypic changes in circulating CD8$^+$ T cells after experimental infection of calves. T cell receptor repertoire together with transcriptomics and epigenomics analyses demonstrated an oligoclonal expansion of infected CD8$^+$ T cells displaying effector and exhaustion gene signatures, including GZMA, GNLY, PD-1, and TOX2 expression. Then, among viral genes expressed in infected CD8$^+$ T cells, we uncovered A10 that encodes a transmembrane signaling protein displaying multiple tyrosine residues, with predicted ITAM and SH3 motifs. Impaired A10 expression did not affect AlHV-1 replication in vitro but rendered AlHV-1 unable to induce MCF. Furthermore, A10 was phosphorylated in T lymphocytes in vitro and affected T cell signaling. Finally, while AlHV-1 mutants expressing mutated forms of A10 devoid of ITAM or SH3 motifs (or both) were able to induce MCF, a recombinant virus expressing a mutated form of A10 unable to phosphorylate its tyrosine residues resulted in the lack of MCF and protected against a wild-type virus challenge. Thus, we could characterize the nature of this γ-herpesvirus-induced PTCL-like disease and identify an essential mechanism explaining its development.

malignant catarrhal fever | CD8$^+$ T cells | transcriptomics | epigenomics | peripheral T cell lymphoma

Significance

Alcelaphine gammaherpesvirus 1 (AlHV-1) is arguably a unique example of perfect coevolution of a virus with its natural host, the wildebeest (*Connochaetes* sp.), resulting in viral persistence in the absence of disease. However, after transmission to phylogenetically related ruminant species, AlHV-1 targets CD8$^+$ T lymphocytes resulting in a deadly peripheral T cell lymphoma, named malignant catarrhal fever (MCF). We previously showed that MCF is induced by the maintenance of viral genomes in T cells, but the exact mechanisms driving MCF were yet unresolved. Our work demonstrated that AlHV-1 infection of calves resulted in dramatic transcriptomic and epigenomic changes in CD8$^+$ T cells. We further identified a viral membrane signaling protein that drives T cell dysregulation and activation, clarifying MCF pathogenesis.

Wildebeest are migratory ungulates (hooved mammals) playing a dominant role in the ecosystem in which they evolve (1), with annual migrations exceeding 1,500 km (2). In East Africa, the Maasai people are herding their livestock in grazing areas of the Serengeti and Maasai Mara plains. The wildebeest migration is an iconic spectacle, but the increasing proximity between wildlife and livestock directly endangers the livelihood of the local herders (3), as cattle are highly susceptible to a fatal viral disease named malignant catarrhal fever (MCF), mainly transmitted by the wildebeest calves born each year.

MCF is an acute and fatal pan-systemic lymphoproliferative disease of a variety of species of ungulates (hooved mammals), including cattle. The main causative agents of MCF are two γ-herpesviruses: ovine gammaherpesvirus 2 (OvHV-2; species *Macavirus ovinegamma2*) and alcelaphine gammaherpesvirus 1 (AlHV-1; species *Macavirus alcelaphinegamma1*). These viruses cause no apparent disease in their natural host species. Sheep are naturally infected by OvHV-2, which is responsible for the sporadic sheep-associated form of MCF. Wildebeest asymptomatically carry AlHV-1, responsible for the wildebeest-derived form of the disease (4, 5). The prevalence of AlHV-1 infection in wildebeest is close to 100%, and transmission mainly occurs during the wildebeest calving period and in the first 3 to 4 mo of life (6–8). The impact of MCF on the local pastoralist populations has largely been underestimated (9–12), and MCF has been reported throughout the world in game farms or zoological collections (13).

Recent reports have demonstrated that AlHV-1 infects and persists in CD8$^+$ T lymphocytes and that the maintenance of the viral genome in these cells via the expression of the latency-associated nuclear antigen (aLANA), encoded by gene ORF73, is essential for MCF induction in the rabbit experimental model (14–20). MCF is characterized by a severe lymphoproliferation of CD8$^+$ T cells in the periphery and infiltration in the perivascular

Author contributions: A.V. and B.G.D. designed research; M.G., F.M., B.Y., J.J., S. Leemans, O.N., W.v.C., S.R., L.M., and B.G.D. performed research; T.v.d.B., A.J.D., T.C., D.V., and S.G. contributed new reagents/analytic tools; M.G., F.M., A.A., G.S.S., S. Li, B.C., B.Y., J.N., L.L., L.G., T.C., and B.G.D. analyzed data; T.v.d.B. acquired funding; and M.G. and B.G.D. wrote the paper.

The authors declare no competing interest.

This article is a PNAS Direct Submission.

[1]M.G. and F.M. contributed equally to this work.

[2]To whom correspondence may be addressed. Email: bgdewals@uliege.be.

This article contains supporting information online at https://www.pnas.org/lookup/suppl/doi:10.1073/pnas.2404536121/-/DCSupplemental.

Published August 1, 2024.

spaces in many organs and tissues of lymphoblastic cells. Thus, MCF resembles a γ-herpesvirus-induced peripheral T cell lymphoma (PTCL) resulting from cross-species transmission from wildebeest to cattle. Related oncogenic human and primate γ-herpesviruses such as Epstein–Barr virus (EBV), Kaposi's sarcoma-associated herpesvirus (KSHV), and saimiriine gammaherpesvirus 2 (SaHV-2) share similarities in the recognized mechanisms of lymphomagenesis (21, 22). However, despite recent work investigating the pathogenesis of wildebeest-derived MCF in cattle and the rabbit experimental model, the mechanisms by which AlHV-1 triggers cell proliferation and activation of latently infected $CD8^+$ T cells to induce a PTCL-like disease remain unresolved (15, 18, 19, 23–28).

Here, we unraveled the nature of the $CD8^+$ T lymphocyte responses induced upon AlHV-1 infection in the target bovine species and revealed how this herpesvirus drives T cell activation, ultimately resulting in the development of MCF lesions and the death of infected animals.

Results

Oligoclonal Expansion of Circulating $CD8^+$ T Cells During MCF. The lack of expression of latency-associated protein aLANA encoded by AlHV-1 ORF73 impairs the induction of MCF in rabbits (19, 24). Here, we validated the complete attenuation of an ORF73-deficient strain (73^{DEL}) in calves upon nasal infection (*SI Appendix*, Fig. S1 *A–D* and Fig. 1 *A–E*). In addition, primary infection of calves with the 73^{DEL} virus fully protected against an intranasal challenge with 10^5 plaque forming unit (PFU) of a virulent wild-type (WT) strain of AlHV-1, further demonstrating that impaired aLANA expression renders AlHV-1 apathogenic and represents an effective strategy for vaccination (Fig. 1 *A–D*). Protection induced by 73^{DEL} virus was revealed by the absence of MCF clinical signs (Fig. 1*B*), lack of infiltration of lymphoblastoid cells in tissues (Fig. 1*C* and *SI Appendix*, Fig. S1*D*), and lack of expansion of $CD8^+$ T cell in peripheral blood mononuclear cells (PBMCs) (Fig. 1 *D* and *E*). However, control WT and Mock/WT groups developed typical MCF in both the infection and challenge phases.

While it remains unknown how AlHV-1 induces MCF lesions, previous results have suggested a nonpermissive infection of $CD8^+$ T lymphocytes leading to their activation and proliferation (14–19, 26). Active division of circulating $CD8^+$ T cells using ex vivo EdU incorporation was further confirmed in samples from calves developing MCF clinical signs (*SI Appendix*, Fig. S1*E*). Such proliferation of $CD8^+$ T cells induced by viral infection could be due to a clonal expansion of infected cells. To test this hypothesis, we analyzed the diversity of the T cell receptor (TCR) of purified circulating $CD8^+$ T cells in calves experimentally infected with AlHV-1 (*SI Appendix*, Fig. S2). Complementary-diversity region 3 (CDR3) sequences of both α and β TCR chains were obtained from calves infected with WT or 73^{DEL} viruses or from mock-infected animals. Group "WT" consisted in a total of six calves that developed MCF during the first infection phase (WT, n = 3) or challenge phase (Mock/WT, n = 3) (Fig. 1*A* and *SI Appendix*, Fig. S1*A*). Calves developing MCF clinical signs showed a reduced TRA and TRB diversity as illustrated by Tree maps (Fig. 1*F* and *SI Appendix*, Fig. S3*C*) and quantified by an increase in the proportion of top 10/20 CDR3 clonotypes (Fig. 1*G* and *SI Appendix*, Fig. S3*A*), a decrease in d25/d50/d75/d90 values (*SI Appendix*, Fig. S3*B*), and associated changes in several diversity and inequality indexes (Fig. 1 *H–J*). This reduced diversity was due to the oligoclonal expansion of private clonotypes from each calf since no increase in the sharing of the TCR repertoire was observed (Fig. 1*K*).

AlHV-1 Infection Induces Activation of $CD8^+$ T Lymphocytes Associated with Effector/Memory and Exhaustion Gene Signatures. We next studied differential gene expression by RNA sequencing sorted peripheral $CD8^+$ T cells from mock-, WT, or 73^{DEL}-infected calves (*SI Appendix*, Fig. S2) (29). Principal component analysis (PCA) and hierarchical clustering revealed that Mock and 73^{DEL} samples clustered together (*SI Appendix*, Fig. S4*A*), whereas WT and Mock/WT samples clustered separately. Samples Mock/WT2 and Mock3 were outliers and were removed from subsequent analyses (*SI Appendix*, Fig. S4*B*). Expression levels of lineage genes in the datasets confirmed the quality of the datasets with high expression of *CD3E*, *CD3D*, *CD8A*, and *CD8B*, whereas low or absent gene expression related to $CD4^+$ T cells, B cells, $WC1^+$ γδ T cells, NK cells, and myeloid cells (*SI Appendix*, Fig. S4*C*). We observed a total of 1,164 upregulated genes in WT samples when compared to Mock samples, and 458 when compared to 73^{DEL} samples, among which 426 were common. In addition, 1,051 genes were significantly downregulated in WT samples when compared to Mock samples and 936 when compared to 73^{DEL} samples, among which 710 were common (*SI Appendix*, Fig. S4 *D* and *E*). Among the top regulated genes in WT samples compared to combined Mock and 73^{DEL} samples, we identified *IRF8, BOLA-DRA, GZMA*, *GZMK, IL15RA, TIGIT, MKI67,* and *TOX2*, whereas we observed downregulation of *NRP1*, *OGT*, and *ITGA5* expression (Fig. 2*A*), suggesting active cell division, sustained cell activation, and potential exhaustion. Gene-set enrichment analysis (GSEA) further revealed significant phenotypic changes in $CD8^+$ T cells during MCF (*SI Appendix*, Fig. S5 *A–C*). In WT samples, we observed significant enrichment of genes involved in IFN-γ response, oxidative phosphorylation and fatty acid metabolism, cell division, apoptosis, mTOR and Myc-targets, immune response to virus infection, TCR signaling, and chromatin remodeling. Genes involved in cell adhesion and TGFβ signaling were significantly enriched in Mock and 73^{DEL} $CD8^+$ T cells.

Among genes involved in TCR signaling, *PDCD1, CTLA4,* and *RHOA* (Fig. 2*B*) and transcription factors like *E2F2, E2F3, BATF, EOMES, PRDM1,* and *TOX2* were upregulated in $CD8^+$ T cells during MCF. Importantly, *TOX2* was among the most significantly upregulated genes in WT samples (Fig. 2*C*), supporting the differentiation to a phenotype related to exhaustion of $CD8^+$ T cells after AlHV-1 infection (30). Moreover, increased *TOX2* and *EOMES* expression was associated with increased *PDCD1*, *LAG3*, *TIGIT,* and *ENTPD1* expression and downregulation of *CD226* expression (Fig. 2 *C* and *D* and *SI Appendix*, Fig. S5*D*). However, *TOX* was not upregulated (*SI Appendix*, Fig. S5*D*). In addition, proliferation marker *MKI67* and *GZMK* were strongly expressed during MCF, whereas signature genes of naive T cells such as *CCR7* and *TCF7* were less expressed in WT samples (Fig. 2*D*). Thus, AlHV-1 infection reprograms circulating $CD8^+$ T cells toward a mixed phenotype of activation, including effector/memory and exhaustion features. Among upregulated genes found in three types of PTCL developing in humans (31), some genes found in PTCL not otherwise specified (PTCL-NOS) were also upregulated during MCF like *PDCD1*, *LAG3,* or *GZMA* (*SI Appendix*, Fig. S5 *E* and *F*). However, no significant similarities in the gene signatures of human PTCL and MCF were clearly identified.

AlHV-1 Infection Results in Specific Chromatin Remodeling in $CD8^+$ T Cells. To further analyze AlHV-1-induced $CD8^+$ T cell reprogramming, we used an assay of transposase-accessible chromatin with high-throughput sequencing (ATAC-seq) to profile

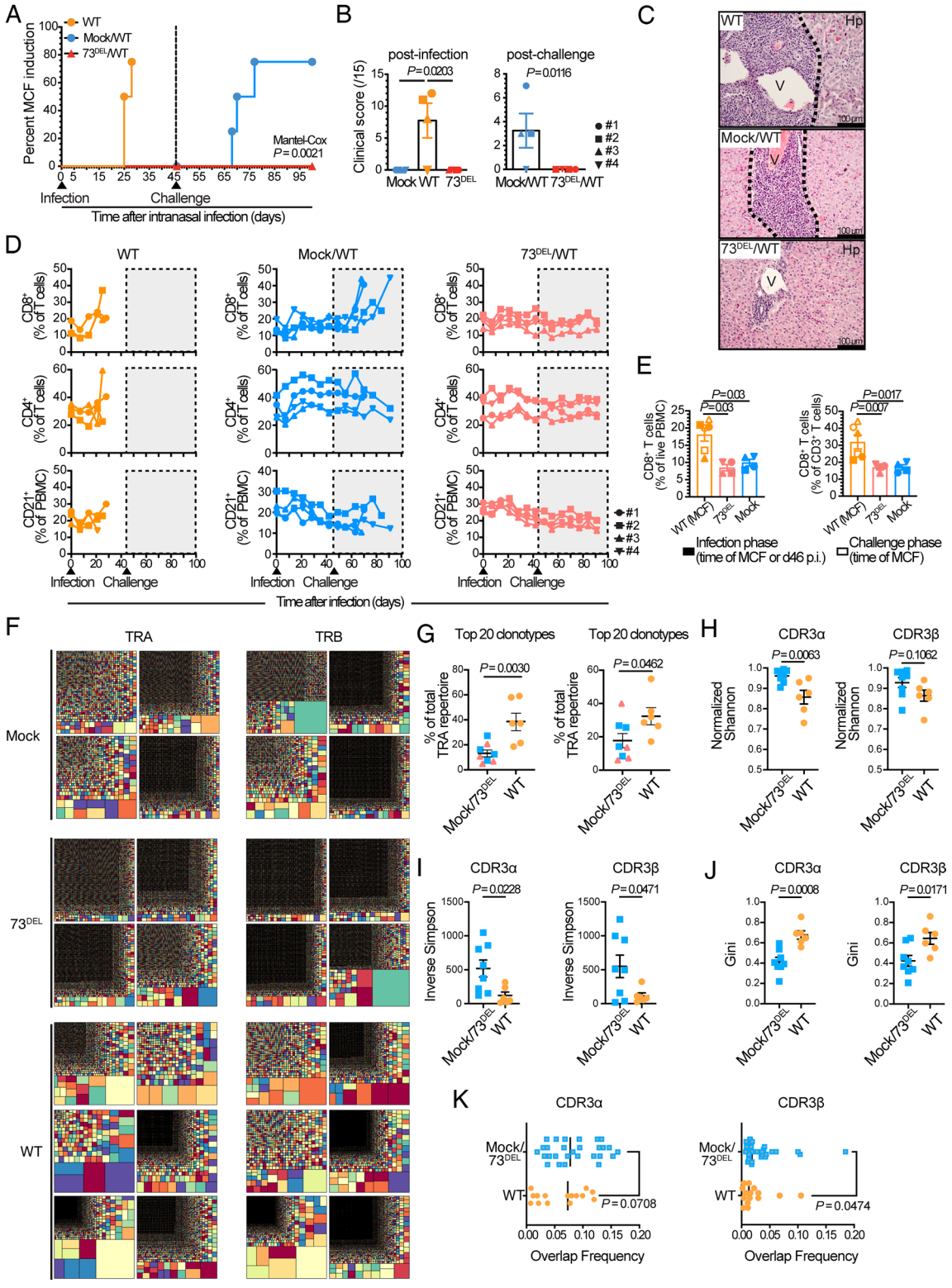

Fig. 1. AlHV-1 73^{DEL} strain protects against WT challenge in bovine, characterized by oligoclonal CD8$^+$ T cell expansion. Calves were inoculated with AlHV-1 WT or 73^{DEL} virus (10^5 PFU, intranasally, n = 4) or a mock inoculum (Mock) and MCF clinical signs were monitored. At day 46 postinfection, calves of the Mock and the 73^{DEL} group were challenged with AlHV-1 WT virus (10^5 PFU, intranasally). (*A*) Percent of MCF induction over time. (*B*) Clinical scores of calves at endpoint. (*C*) Histopathological characterization of MCF lesions. Representative liver sections are shown. Dotted lines areas indicate MCF lesions. Hp, hepatocytes; V, portal veins. (*D*) Proportions of CD8$^+$ T cells, CD4$^+$ T cells, and CD21$^+$ B lymphocytes in PBMCs analyzed by flow cytometry weekly throughout the experiment. Data are plotted for individual calves. Dashed boxes indicate the challenge phase. (*E*) Proportions of CD8$^+$ T cells in PBMCs analyzed by flow cytometry. Data show compiled data from calves at endpoint. (*F*) Representative tree maps of the CDR3 repertoire of each individual calf. Each rectangle represents a unique CDR3 clonotype and its size corresponds to its relative frequency in the repertoire. Data show CDR3α (TRA) and CDR3β (TRB) sequences obtained by TCR-seq. (*G*) Summary data of the proportion occupied by the top 20 clonotypes in both TRA or TRB repertoires. (*H–J*) Summary data of the normalized Shannon diversity (*H*), inverse Simpson diversity (*I*), and Gini (*J*) indexes of CDR3α and CDR3β repertoire. Mock and 73^{DEL} samples were pooled before comparison with WT samples. (*K*) Repertoire sharing measured as overlap frequencies of both CDR3α and CDR3β sequences. Each symbol represents one individual calf. Bar indicates mean ± SEM. Statistical significance was calculated using one-way ANOVA or Kruskal–Wallis test and Sidak's or Dunn's posttest for multiple comparisons, or unpaired Student's *t* test. *P* indicates *P*-value.

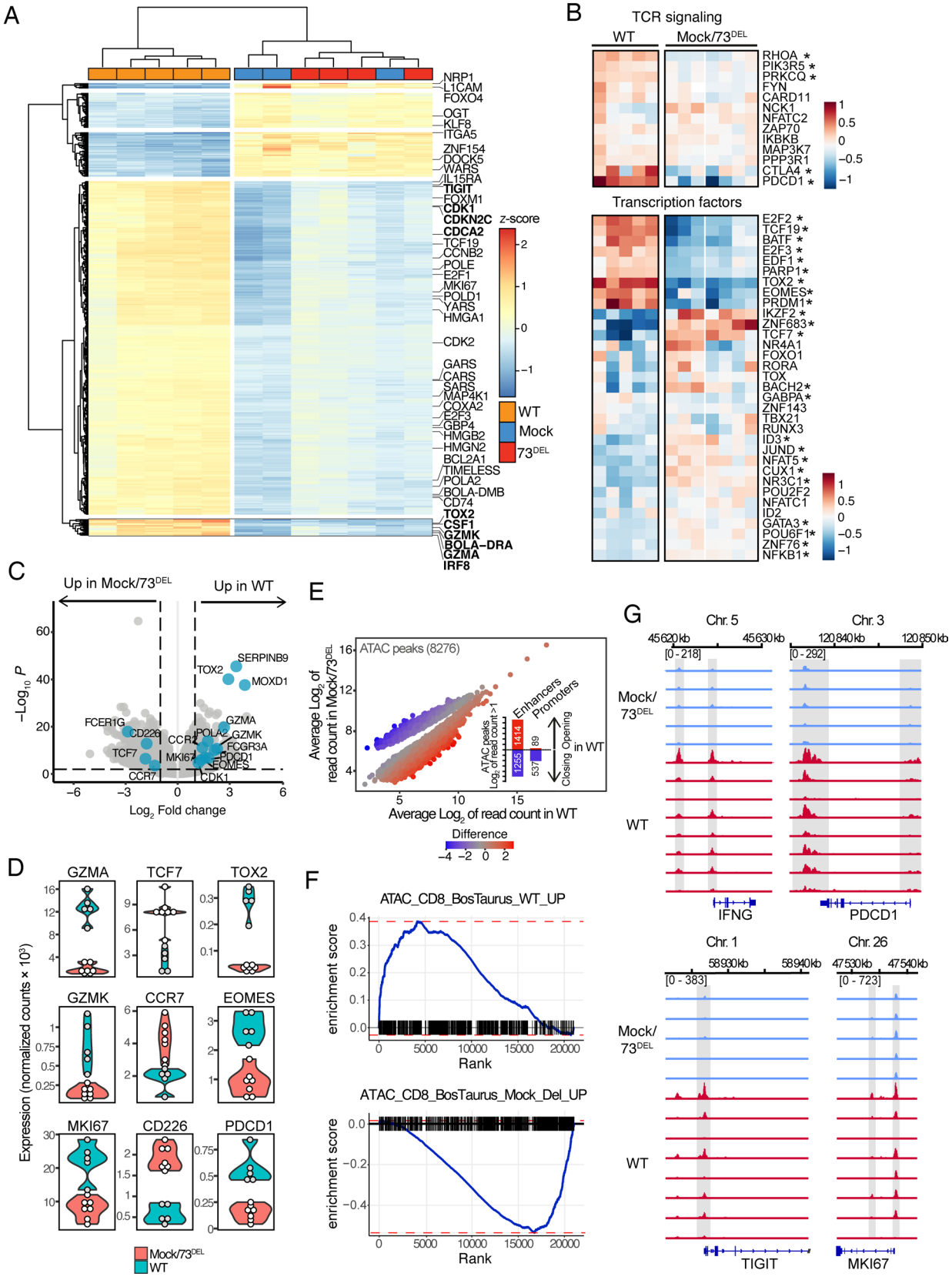

Fig. 2. Transcriptomic and chromatin availability analyses reveal mixed gene signature of effector-memory and exhaustion in circulating bovine CD8$^+$ T lymphocytes during MCF. (*A–D*) Bulk RNA-seq was performed on CD8$^+$ T lymphocytes. (*A*) Unsupervised hierarchical clustering of the top 500 differentially expressed genes (DEG). Biologically relevant genes are listed. Heatmap color scale indicates *z*-score. (*B*) Heatmap of the expression levels of curated genes associated with TCR signaling and transcription factors. Stars indicate significant difference ($P < 0.05$) of expression between WT and Mock/73^{DEL}. (*C*) Volcano plot of differential gene expression between WT and Mock/73^{DEL} samples. Curated gene dots are indicated in green. (*D*) Gene expression as normalized read counts of indicated genes in WT and Mock/73^{DEL} samples. (*E–G*) Bulk ATAC-seq analysis of CD8$^+$ T lymphocytes. (*E*) Mean log2 ATAC-seq peak atlas of DOR for WT (red) and Mock/73^{DEL} (blue). Histograms indicate the distribution of DOR at promoters and enhancers with a difference in log2 read count >1. (*F*) GSEA plot showing enrichment score of DORs in WT and in Mock/73^{DEL}. (*G*) Representative tracks of DORs in WT CD8$^+$ T cells (highlighted in gray) showed on IGV genome browser.

the open-chromatin landscape of sorted CD8$^+$ T lymphocytes isolated from MCF-developing calves (WT) or from Mock and 73^{DEL}-infected calves. CD8$^+$ T cells were sort-purified from cryopreserved PBMC samples obtained from this experiment and from a previous study (19). An atlas was created containing all obtained peaks (73,497 peaks). PCA on this atlas showed two separated clusters of WT and Mock/73^{DEL} with 28% of variance explained by PC1 (*SI Appendix*, Fig. S6*A*). DESeq2 was used with a *P*-adjusted cutoff of 0.05 to identify a total of 8,276 differentially opened regions (DOR). These regions were further filtered by choosing the ones with a minimum difference of 1 in average Log2 reads count between the two conditions, resulting in 1,503 DORs in WT and 1,792 DORs in Mock/73^{DEL} groups, respectively, with a high proportion of these regions located in enhancers (Fig. 2*E*). We then assessed the chromatin accessibility within peaks annotated to DEG obtained from RNA-seq analysis and showed as expected that DEGs from WT are more accessible in WT compared to samples from Mock/73^{DEL} and vice versa (*SI Appendix*, Fig. S6*B*). To verify the association between chromatin accessibility and gene expression, a GSEA approach was performed. Using the RNA-seq results as a dataset, a significant enrichment of the annotated DORs identified in WT and Mock/73^{DEL} conditions was identified such as *IFNG*, *PDCD1*, *TIGIT,* and *MKI67* in WT, and *CD226*, *TCF7*, *CCR7,* and *ITGA5* in Mock/73^{DEL} (Fig. 2 *F* and *G* and *SI Appendix*, Fig. S6 *C*–*E*). In addition, we found that DORs in WT significantly enriched binding motifs for T-BOX (EOMES and TBX21), RUNX, IRFs, and STATs transcription factors (*SI Appendix*, Fig. S6 *F* and *G*). Hence, AlHV-1 infection leads to a reorganization of the chromatin landscape in CD8$^+$ T lymphocytes.

AlHV-1 Infection Is Mainly Detected in EOMES- and TOX2-Expressing CD8$^+$ T Cells. To further characterize the transcriptomic heterogeneity of CD8$^+$ T cell responses during MCF, we performed single-cell RNA sequencing (scRNA-seq) of CD8$^+$ T cells purified from the cryopreserved PBMC of two mock-infected and MCF-developing calves. Eleven different clusters were identified, among which clusters C2, C3, C5, and C6 were enriched during MCF (Fig. 3 *A* and *B*). Signature genes of naive T cells such as *CCR7, TCF7,* and *LEF1* were enriched in cluster C0 (Fig. 3 *C* and *D* and *SI Appendix*, Fig. S7), whereas cluster C1 did not show a specific signature with upregulation of transcripts of *IL7R, S100A13,* and *S100A4* and was mainly present in the Mock sample. Cluster C2 showed signature genes of effector/activation like *CX3CR1, CCL5, BOLA, GNLY,* and type I IFN response such as *OASL, ISG20, IRF1,* and *IRF9*. Cluster C3 was mainly present during AlHV-1 infection and was characterized *GZMM, PDCD1, TOX2, LAG3, GNLY, NKG7,* and *BCL2A1* expression. Cells grouped in C4 expressed natural killer (NK)-related genes such as *KIR2DL5A, FCER1G, IKZF2,* and *KLRD1.* Cluster C5 contained cells expressing effector/memory genes such as *GNLY, PTPRC, ITGA4, MKI67,* and *NKG7* suggesting terminally effector T cells (32). Cluster C6 was characterized by the expression of genes associated with exhaustion and proliferation such as *LAG3*, *PDCD1*, *TIGIT*, *TOX2, CCNB1,* and *MKI67.* Cluster C7 included genes such as *IL2RA*, *CD69,* and *BHLEH40*. Cells in cluster C8 expressed genes such as *ID3* and *IKZF2* and seem to represent a population transiting between C0 to C4. The few cells forming cluster C9 upregulated *CD163L* and *RHEX* and cluster C10 was composed of very few cells. AlHV-1-specific RNA reads were extracted from the scRNA-seq data using Viral-Track (33). Viral transcripts were detected in a total of 34 cells, which clustered together mainly in C6 (Fig. 3*E*). Thus, C6 could represent a niche of AlHV-1 infected cells. Importantly, RT-qPCR on low cell number inputs revealed that one cell out of 25 circulating CD8$^+$ T cells expressed detectable viral RNA (*SI Appendix*, Fig. S8 *A*–*C*), suggesting that scRNA-seq data underestimates the proportion of infected cells. Signature genes involved in proliferation, effector functions, memory, and activation/exhaustion phenotype were enriched in C3, C5, and C6 (Fig. 3*D*). Thus, AlHV-1 infection of CD8$^+$ T cells likely results in severe cellular reprogramming.

Then, a subset of the three clusters enriched during MCF and in which viral RNA could be detected was created (Fig. 3 *F* and *G*). Interestingly, trajectory analysis was performed, highlighting C6 as a branching point of C3 and C5 (Fig. 3*H*). At the single-cell level, we also observed that the relative abundance of larger TCR clonotype groups was higher in CD8$^+$ T cells upon AlHV-1 infection and combined single-cell TCR-sequencing analysis showed that the more expanded clonotypes were found in clusters C3, C5 and C6 (*SI Appendix*, Fig. S9 *A* and *B*), with C3 sharing substantial TCR sequences with C5 and C6. However, infected cells identified by scRNA-seq (Fig. 3*E*) expressed a diverse range of TCR (*SI Appendix*, Table S1), suggesting that while AlHV-1 induces an oligoclonal expansion of CD8$^+$ T cells, viral infection does not target specific TCR clonotypes, which is in line with the bulk TCR-seq data (Fig. 1*K*).

Selective Transcription of the Viral Genome in Infected Bovine CD8$^+$ T Cells. Sequence reads obtained from the RNA-seq data of purified CD8$^+$ T cells (*SI Appendix*, Fig. S2*A*) were mapped on the viral genome (Fig. 4*A*). RNA-seq analysis revealed an expected low level of expression, ranging from 2.9×10^{-4} to 2.4×10^{-2} percent of reads mapping on AlHV-1 genome for the overall libraries (Fig. 4*B*), whereas AlHV-1 genome was transcribed at similar levels when compared to the bovine genome (Fig. 4*C*). These results suggest a low but consistent viral RNA expression in infected cells. Importantly, we confirmed the absence of detection or very low expression of genes encoding proteins indispensable for lytic replication such as viral DNA polymerase (ORF9), the major capsid protein (ORF25), and the major tegument protein (ORF64). Among AlHV-1-specific genes, RNA expression of the coding sequences of A2, A3, A4, A4.5, A6, A9, A9.5, and A10 was observed. Little or no expression of A5, A7, or A8 was detected, suggesting that the viral G protein-coupled receptor encoded by A5 and the gp42/gp350-homolog envelope proteins encoded by A7 and A8 are not expressed in T lymphocytes during MCF (25, 26). However, expression of the essential envelope glycoprotein B (ORF8) was detected, likely explaining the detection of anti-AlHV-1 antibodies (*SI Appendix*, Fig. S1*C*). These results demonstrate the expression of selective regions across AlHV-1 genome, including protein-encoding genes that were involved in CD8$^+$ T cell reprogramming and MCF lesions.

A10 Gene Expression Is Essential for MCF Induction. Among viral genes found to be expressed in CD8$^+$ T cells during MCF (Fig. 4*A*), A4 and A10 might be involved in T cell reprogramming. Indeed, based on predictive analyses, A4 is a potential ortholog of the oncogene STP encoded by SaHV-2 (34). In addition, A10 encodes a putative transmembrane protein sharing sequence similarities with the oncoprotein TIP of SaHV-2, including a predicted immunoreceptor tyrosine-based activation motif (ITAM) and an SRC homology 3 (SH3) domain. To determine whether either or both of A4 or A10 are involved in MCF pathogenesis, recombinant viruses were generated to impair the expression of either or both of A4 or A10. First, a nonsense mutation was inserted in the coding sequence of A4 to generate a A4^{STOP} virus (*SI Appendix*, Fig. S10 *A* and *B*). The A4^{STOP} virus could replicate efficiently in vitro

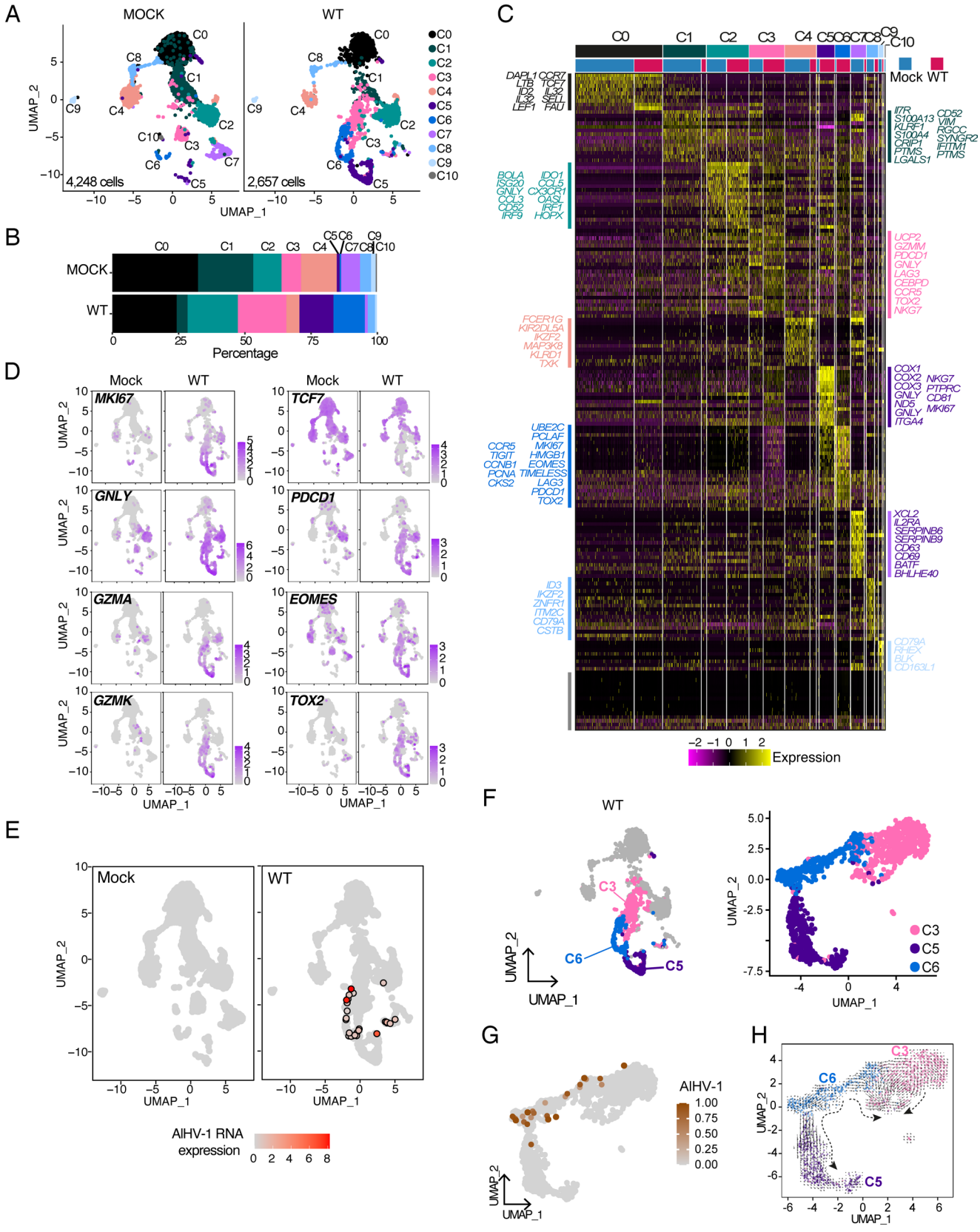

Fig. 3. scRNA-seq of circulating bovine CD8$^+$ T lymphocytes during MCF. ScRNA-seq was performed on cryopreserved CD8$^+$ T lymphocytes at endpoint from a mock-infected calf or from a calf developing MCF. (*A*) Split UMAP visualization of combined single CD8$^+$ T cell transcriptomes of WT or Mock-infected calves, with unsupervised Seurat clustering analysis. (*B*) Proportions of each cluster in each dataset. (*C*) Differential gene signatures. Curated genes are highlighted for each cluster. (*D*) FeaturePlot of expression of selected genes. (*E*) ViralTrack analysis of AIHV-1 RNA expression, plotted on the UMAP visualization. Scale is represented as a heatmap of the level of viral RNA expression. Each virus-positive cell is identified with a circle. (*F*) Unsupervised Seurat clustering of clusters 3, 5, and 6 as a subset of the global dataset. (*G*) FeaturePlot of expression of AIHV-1 RNA expression in C3, C5, and C6. (*H*) RNAVelocity trajectory analysis.

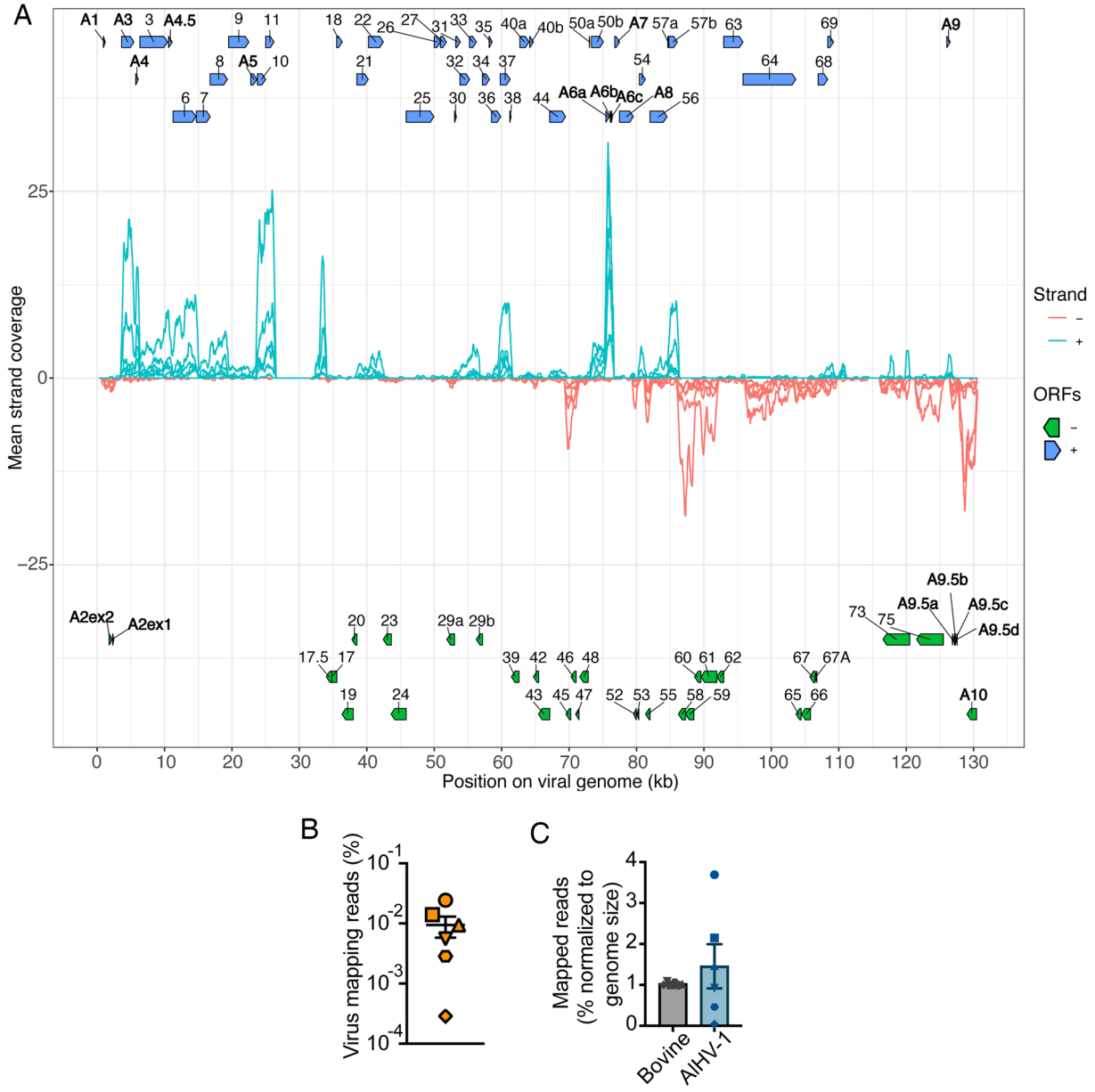

Fig. 4. Genome-wide viral RNA expression in circulating CD8$^+$ T lymphocytes during MCF. (*A*) Coverage plot of AlHV-1 RNA expression across the viral genome. Each curve represents an individual calf. Green and red lines represent forward or reverse strands, respectively. Arrowed indicate predicted ORFs. "A" prefix refers to AlHV-1-specific genes. (*B*) Percentage of viral reads relative to the total number of reads for each sample. (*C*) Percentage of bovine and viral mapped reads normalized on the bovine or AlHV-1 genome size, respectively.

and induce MCF in the rabbit experimental model (*SI Appendix*, Fig. S10 *C*–*G*). Thus, A4 is not involved in MCF induction. Then, we generated two complementary mutant viruses impaired for A10 expression. The entire A10 coding sequence was deleted to generate an A10^{DEL} virus, and a nonsense mutation inserted in the coding sequence of A10 to create the A10^{STOP} virus (Fig. 5 *A* and *B*). Although the A10^{DEL} and A10^{STOP} viruses replicated efficiently in vitro (Fig. 5 *C* and *D*), both were unable to induce hyperthermia in infected rabbits (Fig. 5*E*), and all rabbits survived the infection except for animals infected with the WT virus, which developed MCF clinical signs and lesions (Fig. 5*F*). The lack of A10 expression resulted in the absence of splenomegaly and adenomegaly (Fig. 5*G*), no expansion of CD8$^+$ T cells (Fig. 5*H*), and no infiltration of lymphoblastoid cells in tissues (Fig. 5*I*). Interestingly, while the viral DNA load strikingly increased after infection with the WT virus, few or no viral copies were detected in PBMC after infection with the A10^{DEL} and A10^{STOP} viruses (Fig. 5*J*). Finally, specific anti-AlHV-1 antibodies were detected in all infected rabbits (Fig. 5*K*). These results demonstrate that A10 expression is essential for MCF induction, which was further confirmed with a double A4^{STOP}A10^{STOP} recombinant virus (*SI Appendix*, Fig. S10).

Phosphorylation of Tyr Residues in A10 Is Required for MCF, but ITAM and SH3 Domains Are Not. A10 is predicted to encode a 472 amino acid transmembrane signaling protein (Fig. 6*A*), in which the intracytoplasmic domain contains an ITAM, a SH3 domain, and 13 tyrosine (Tyr or Y) residues. Stable expression of a tagged form of A10 protein fused with two Flag (DYKDDDK) motifs revealed that A10 is constitutively phosphorylated in Jurkat cells (Fig. 6*B*). To further explore how A10 would signal in infected T cells to modulate T cell activation, we generated vectors expressing mutated forms of A10 for the ITAM (A10 ITAM^{mut}), the SH3 domain (A10 SH3^{mut}), the Tyr residues replaced by phenylalanine residues (Phe or F; A10$^{Y\text{-}13\times\text{-}F}$), and

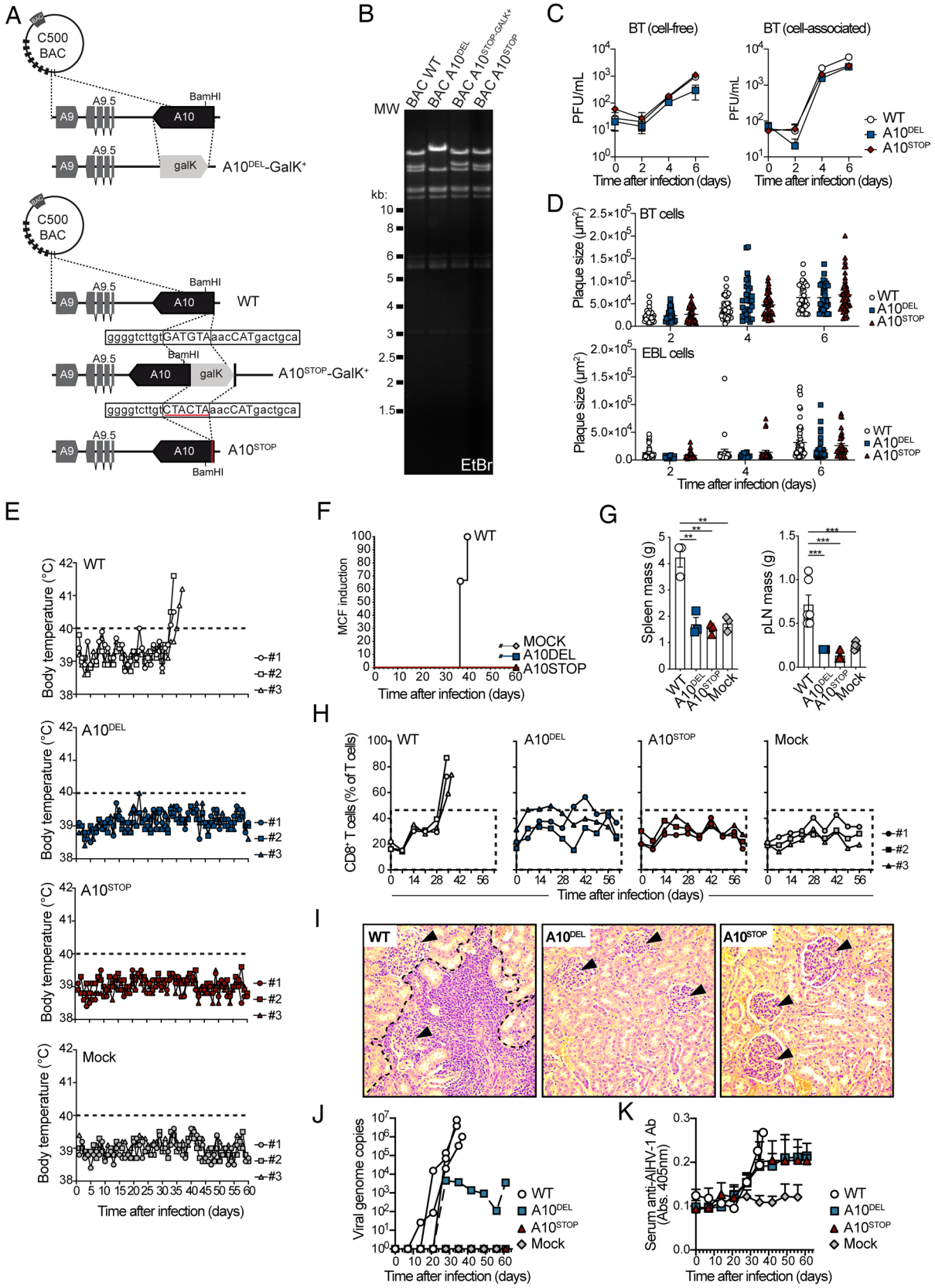

Fig. 5. A10 expression is dispensable for AlHV-1 propagation in vitro but is essential for MCF induction. (*A*) Generation of the A10^{DEL} and A10^{STOP} viruses. (*B*) Restriction profiles of the obtained constructs, after BamHI digestion and electrophoresis. EtBr: ethidium bromide. (*C*) Multistep growth curves. Cell-free and cell-associated infectivity viral titers are shown. Mean ± SD. (*D*) Infectious plaque areas. Mean ± SD. (*E*) Body temperature overtime. (*F*) Percent of MCF induction over time. (*G*) Spleen and popliteal lymph node (pLN) mass at time of sacrifice. Mean ± SEM. (*H*) Proportions of CD8$^+$ T cells in PBMCs analyzed by flow cytometry. (*I*) Histological characterization. Kidney sections of one rabbit representative of each group are shown. Arrows indicate renal corpuscles. (*J*) Viral genome copies in PBMCs overtime. RT-PCR quantification was normalized on 10^5 copies of cellular β-globin. (*K*) AlHV-1-specific antibodies in the serum as measured by indirect ELISA. (*D*, *E*, *G*, and *H*) Individual measurements are shown. One-way ANOVA with Sidak's post hoc test was used to identify significant differences (*$P < 0.05$, **$P < 0.01$, ***$P < 0.001$).

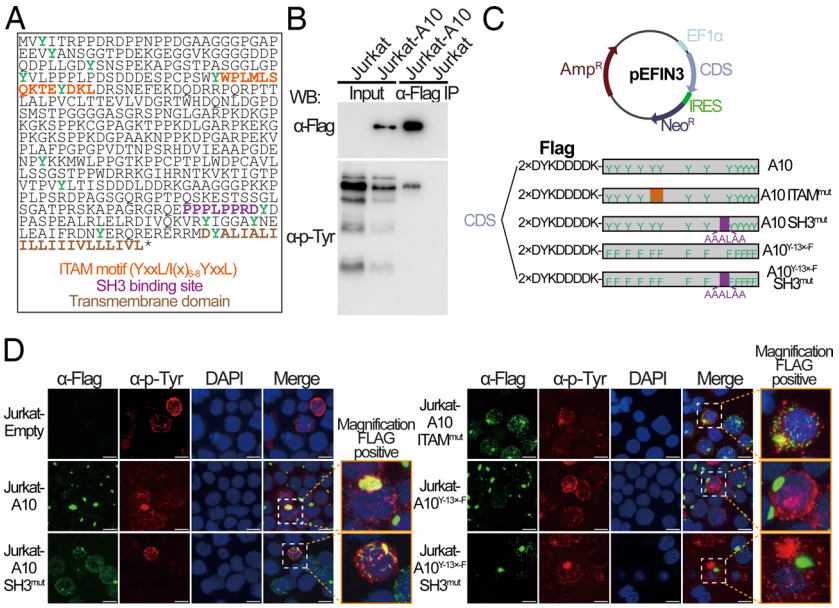

Fig. 6. A10 encodes a phosphorylated transmembrane protein. Jurkat stable cell lines were generated by transfecting linearized expression vectors followed by geneticin positive selection. (*A*) Peptidic sequence of A10 highlighting ITAM motif, SH3, and transmembrane domains. Tyrosine residues are highlighted in bold green. (*B*) Anti-FLAG immunoprecipitation of Jurkat or Jurkat-A10 cell lines, followed by immunoblotting specific for FLAG and phospho-Tyr. (*C*) Expression vectors of mutated forms of A10 in plasmid vector pEFIN3. Mutated A10 coding sequences are transcribed as a polycistronic RNA, separated from a neomycin resistance gene by an internal ribosome entry site (IRES). (*D*) Confocal analysis after cytospin of Jurkat cells followed by anti-FLAG and anti-phospho-Tyr co-staining. Nuclei are stained with DAPI. (Bars, 50 μm.)

both the SH3 domain and Tyr residues (A10$^{Y\text{-}13\times\text{-}F}$-SH3^{mut}) (Fig. 6*C*). Confocal microscopy revealed that A10 forms clusters in Jurkat-A10 cells (Fig. 6*D*), as previously observed for SaHV-2 TIP protein (35), whereas the ITAM and SH3 mutations disrupted the subcellular localization of A10. Phosphorylated Tyr residues colocalized with Flag-specific signals in Jurkat-A10, Jurkat-A10 ITAM^{mut}, and Jurkat-A10 SH3^{mut} cells. However, phosphorylated Tyr residues did not colocalize with the Flag-specific signal in Jurkat-A10$^{Y\text{-}13\times\text{-}F}$ or Jurkat-A10$^{Y\text{-}13\times\text{-}F}$-SH3^{mut} cells, demonstrating effective knock-in mutations of phospho-Tyr residues (Fig. 6*D*). In vitro restimulation with increasing concentrations of anti-CD3 (*SI Appendix*, Fig. S11*A*) resulted in significant upregulation of the T cell signaling activation marker CD69 in Jurkat-A10, when compared to the Jurkat cell lines expressing the A10$^{Y\text{-}13\times\text{-}F}$ mutants (*SI Appendix*, Fig. S11 *A* and *B*). Moreover, WT A10 expression in Jurkat drove increased expression of GZMA and GNLY (*SI Appendix*, Fig. S11*C*). Thus, these results demonstrate that Jurkat-A10 cells have altered T cell signaling and display an activation phenotype, which was not observed in Jurkat-A10$^{Y\text{-}13\times\text{-}F}$ or Jurkat-A10$^{Y\text{-}13\times\text{-}F}$-SH3^{mut} transduced cell lines. Then, AlHV-1 recombinant viruses were generated to express A10 mutant forms devoid of ITAM or SH3 motifs as well as expressing the A10$^{Y\text{-}13\times\text{-}F}$-SH3^{mut} knock-in gene (*SI Appendix*, Fig. S12 *A–D*). Importantly, the absence of a functional ITAM or SH3 domain in A10 did not significantly affect the development of MCF upon rabbit infection (Fig. 7 *A* and *B* and *SI Appendix*, Fig. S13), indicating that these elements are dispensable for driving MCF induction. In contrast, while recombinant AlHV-1 A10$^{Y\text{-}13\times\text{-}F}$-SH3^{mut} virus did not show any growth defect in vitro (*SI Appendix*, Fig. S12 *E* and *F*), rabbit infection with the A10$^{Y\text{-}13\times\text{-}F}$-SH3^{mut} virus did not result in MCF clinical signs, hyperthermia (Fig. 7*C*), CD8$^+$ T cell expansion in PBMCs, spleen and pLN (Fig. 7 *D* and *G*), enlargement of spleen and lymph nodes (Fig. 7*H*), lymphoblastoid cells in the tissues (Fig. 7*I*), or significant viral genome detection (Fig. 7 *J* and *K*). In addition, when rabbits infected with the AlHV-1 A10$^{Y\text{-}13\times\text{-}F}$-SH3^{mut} virus were challenged with the pathogenic AlHV-1 WT virus, the animals did not develop MCF (Fig. 7 *E–I*), suggesting that mutation of A10 does not impair protective immunization. Thus, phosphorylation of Tyr residues in the A10 protein is a part of the mechanism driving MCF development in vivo.

Discussion

MCF is a lymphoproliferative disease that can develop in several species of hooved mammals of the subfamilies *Bovinae* and *Cervidae* and is induced by cross-species transmission of certain herpesviruses in the *Macavirus* genus (4). Among these viruses, AlHV-1 is the most studied as it is able to replicate in cell culture and can induce MCF experimentally in susceptible animal species. However, AlHV-1 infection does not induce major clinical signs or lesions in its natural host, the wildebeest, suggesting a high degree of adaptation of the virus to its host during coevolution. Thus, it appears likely that AlHV-1 has evolved mechanisms to persist in wildebeest, whereas transmission to related animal species can result in the development of a deadly disease via a mechanism involving latent infection of CD8$^+$ T lymphocytes that induces cell proliferation and activation (14–20). However, the exact nature of CD8$^+$ T cell responses to AlHV-1 infection and the virus-driven mechanisms resulting in CD8$^+$ T cell activation remained largely unknown.

This study demonstrates that AlHV-1 infection in cattle drives the oligoclonal expansion of CD8$^+$ T lymphocytes. Analysis of the TRA and TRB repertoire highlighted the significant loss of TCR diversity in calves developing MCF that was due to the oligoclonal expansion of private clonotypes. Although we still do not know how AlHV-1 enters CD8$^+$ T cells, these findings show that the expansion of CD8$^+$ T cells is likely explained by clonal proliferation of multiple infected cells. The nature of the expansion of CD8$^+$ T cells during MCF was further revealed by (sc-)RNA-seq and ATAC-seq, which identified a unique gene signature associated with mixed effector/memory and exhaustion features, including the upregulation of *TOX2*, *EOMES*, *PDCD1*, *GZMA*, *GNLY*, and *GZMK*. Importantly, expansion was only observed upon

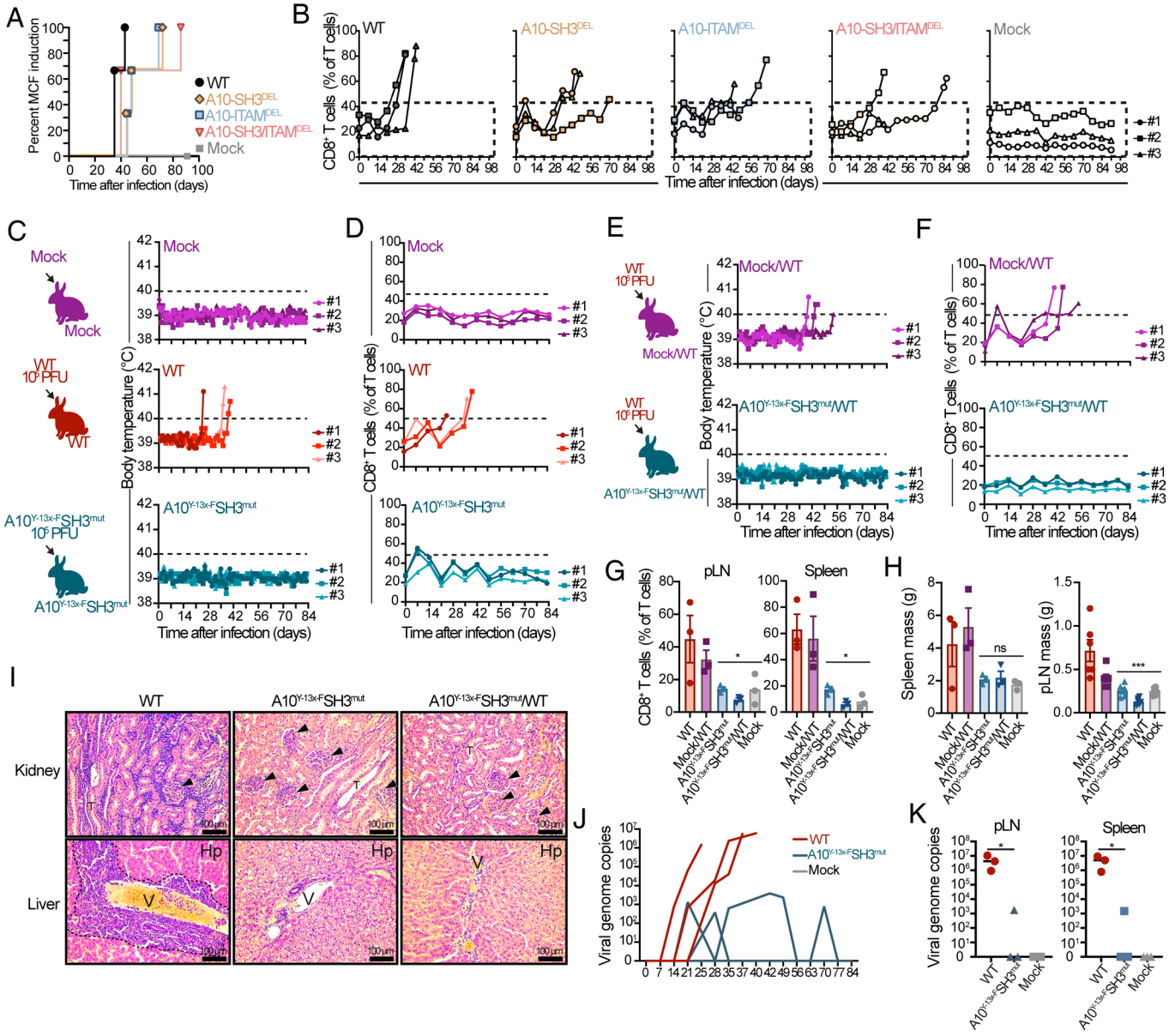

Fig. 7. A10 phosphorylation is essential for MCF induction but independently of ITAM and SH3 motifs. (*A* and *B*) MCF induction (*A*) and proportions of CD8$^+$ T cells in PBMCs (*B*) rabbits infected with WT, A10-ITAM^{DEL}, A10SH3^{DEL}, or A10-ITAM/SH3^{DEL} virus strains or mock-infected. (*C* and *D*) Body temperature overtime (*C*) and proportions of CD8$^+$ T cells in PBMCs (*D*) after intranasal inoculation of media (Mock), WT, or A10$^{Y\text{-}13\text{-}F}$SH3^{mut} virus strains. (*E* and *F*) Body temperature overtime (*E*) and proportions of CD8$^+$ T cells in PBMCs (*F*) after intranasal WT challenge of the mock or A10$^{Y\text{-}13\text{-}F}$SH3^{mut}-infected rabbits in panel (*C*). (*G*) Proportions of CD8$^+$ T cells in pLN and spleen at time of euthanasia. (*H*) Spleen and pLN mass at time of euthanasia. (*I*) Histological characterization. Representative kidney and liver sections are shown. (*J* and *K*) Viral genome copies after inoculation as in (*C*) in PBMCs over time (*G*) or in pLN and spleen at time of euthanasia (*H*). RT-PCR quantification was normalized on 10^5 copies of the cellular β-globin gene sequence. Data are plotted as individual measurements. Mean ± SEM. One-way ANOVA with Sidak's post hoc test was used to identify significant differences (*$P < 0.05$, ***$P < 0.001$).

infection with a virus able to maintain its genome in the infected cells. The canonical T cell exhaustion regulator *TOX* was not upregulated (36–39), but *TOX2* may also drive T cell exhaustion or chromatin accessibility of follicular T cells in mice as well as regulate natural killer cell fate in human (40–42). Although it remains unclear how *TOX2* is activated, our findings highlighted profound transcriptomic changes during MCF as well as significant differences in open chromatin regions with enriched T-box (*EOMES*, *TBX21*, and *RUNX2/3*) or *IRFs* transcription factors motifs, demonstrating that AlHV-1 infection drives specific activation pathways in T lymphocytes.

Although viral RNA could not be detected in all CD8$^+$ T cells of MCF-specific clusters C3 and C6, we previously demonstrated that a majority of CD8$^+$ T cells carry the viral genome during MCF (19). It is possible that a small fraction of infected cells would activate uninfected CD8$^+$ T cells in a bystander fashion, but it appears more likely that the level of viral gene expression remains low and undetectable by scRNA-seq in many cells. Supporting this hypothesis, bulk RNA-seq only identified a small fraction (a maximum of 2.4×10^{-2} percent) of viral sequences mapping on the AlHV-1 genome, whereas low cell number input RT-qPCR identified 1 infected CD8$^+$ T cells out of 25. An additional nonexclusive hypothesis could be a "hit and run" phenomenon where AlHV-1 infection would sustainably reprogram T lymphocytes that would then lose viral epigenomes while proliferating. Coverage analysis revealed that a number of specific regions of the viral genome were expressed. Genes A1, A5, A7, and A8 were barely transcribed in CD8$^+$ T cells, and it was already known that A2, A3, and A5 are

not essential for MCF (25, 27, 28). Among these detected viral RNAs, genes A4.5 and A9 are viral Bcl-2 homologs and might regulate cell survival and hence lymphomagenesis. However, EBV also encodes two viral Bcl-2 homologs that have been shown to be dispensable for B cell proliferation once latency is established (43). A6 encodes a b-ZIP protein that is thought to regulate the shift from latency to replication, while A9.5 encodes a viral secreted protein having some sequence similarities with interleukin 4, although its function during MCF remains unknown (44, 45). We learned further from viral RNA read coverage from RNA-seq analysis that infected $CD8^+$ T cells express genes that tend to be associated with latent or abortive replication rather than lytic replication, thus confirming our previous findings (15, 16, 19).

We further focused our attention on two putative oncogenes based on their positional and sequence homology to other herpesviruses. We identified A4 and A10 as putative homologous to SaHV-2 oncogenes STP and TIP, respectively (22, 46), and having homologs in the OvHV-2 genome (47, 48). Impaired expression of A4 or A10 (or both) did not significantly affect viral growth in vitro, suggesting that both genes are dispensable for viral replication. Interestingly, the lack of A4 expression did not affect the induction of MCF upon infection of rabbits and induced MCF-related hyperthermia with a shorter delay compared to the WT virus. However, when A10 expression was impaired during infection in vivo, either by complete deletion of the protein-coding sequence or by insertion of an in-frame nonsense mutation, the virus was nonpathogenic and unable to induce MCF. These observations highlighted the role of the A10 signaling protein in the induction of MCF, potentially via interacting with the T cell signaling pathway leading to persistent T cell activation. The SaHV-2 TIP oncoprotein has been shown to make lipid rafts on the cell membrane and interact with Lck and Zap-70 in transduced T lymphocytes (35, 46, 49, 50), which is similar to our observations while studying A10 protein expression in the Jurkat cell lines. Surprisingly deletion from the viral genome of the predicted ITAM or the SH3 domain (or both) did not affect the induction of MCF upon infection, while mutation of ITAM/SH3 sequences disrupted subcellular localization in Jurkat cells. The observations that the A10 putative ITAM or SH3 domain are not essential to induce MCF but likely alters lipid-raft formation rather suggest that these putative elements might play a role in the regulation of T cell activation during infection in the natural host, the wildebeest. However, when the thirteen Tyr residues were mutated to Phe in the $A10^{Y\text{-}13\times\text{-}F}$ mutant protein, the resulting protein localized as clusters likely at the surface of Jurkat cells like the native A10 protein, and when AlHV-1 expressed this mutated form of A10, the virus was unable to induce MCF. Thus, these results indicate a determinant role of A10 phosphorylation in infected $CD8^+$ T cells that ultimately drives the peripheral T cell lymphomagenesis observed during MCF.

What remain unknown are the molecular partners of phosphorylated A10 involved in T cell reprogramming, leading to the observed expansion and activation. However, our findings indicate that MCF results from an alteration of T cell signaling in infected $CD8^+$ T cells, leading to the lymphoproliferation of activated/exhausted T cells in which A10 and its phosphorylation play an essential role.

Materials and Methods

Ethics statement, cell lines and viruses, animals and viral infection, PBMC preparation, antibodies and flow cytometry, $CD8^+$ T cell isolation, RNA extraction, RNA-seq and analysis, TCR-sequencing and CDR3 sequence analysis, ATAC-seq, scRNA-seq and single-cell VDJ analysis, production of recombinant virus strains, viral growth curves and plaque size assay, quantification of viral genomes and cDNA synthesis for RT-PCR, antibody ELISA, histological analysis, plasmid construction, Jurkat cell transduction and establishing stable cell lines, confocal analysis, Western blot and immunoprecipitation, and statistical analysis are described in *SI Appendix, Materials and Methods*.

Data, Materials, and Software Availability. Sequencing data have been deposited in NCBI Genbank (GSE253729) (29). All other data are included in the manuscript and/or supporting information.

ACKNOWLEDGMENTS. We are thankful to the technician and administrative team of the Department of infectious and parasitic diseases, to B. Machiels for insightful discussions, to members of the GIGA Genomics platform, and to A. Chasseur for contributing to the generation of the $A4^{STOP}$ recombinant virus. We are also grateful to H. Li and C. Cunha for providing reagents for competitive inhibition enzyme-linked immunosorbent assay (ELISA).

Author affiliations: [a]Department of Infectious and Parasitic Diseases, Faculty of Veterinary Medicine—Fundamental and Applied Research for Animals & Health (FARAH), University of Liège, Liège 4000, Belgium; [b]Institute for Medical Immunology, Université Libre de Bruxelles, Gosselies 6041, Belgium; [c]Center for Research in Immunology, Université Libre de Bruxelles, Gosselies 6041, Belgium; [d]Department of Pharmacotherapy and Pharmaceutics, Université Libre de Bruxelles, Brussels 1050, Belgium; [e]Walloon Excellence in Life Sciences and Biotechnology (WELBIO), WEL Research Institute, Wavre 1300, Belgium; [f]Groupe Interdisciplinaire de Génoprotéomique Appliquée (GIGA), GIGA-Genomics core facility, University of Liège, Liège 4000, Belgium; [g]Medical Research Council (MRC)-University of Glasgow Centre for Virus Research, Glasgow G61 1QH, United Kingdom; [h]The Roslin Institute, The Royal (Dick) School of Veterinary Studies, University of Edinburgh, Easter Bush, Midlothian EH25 9RG, United Kingdom; and [i]Sciensano, Scientific Directorate Infectious Diseases in Animals, Experimental Center Machelen, Machelen 1830, Belgium

1. M. J. Kauffman *et al.*, Mapping out a future for ungulate migrations. *Science (1979)* **372**, 566–569 (2021).
2. C. J. Torney, J. G. C. Hopcraft, T. A. Morrison, I. D. Couzin, S. A. Levin, From single steps to mass migration: The problem of scale in the movement ecology of the Serengeti wildebeest. *Philos. Trans. R. Soc. B: Biol. Sci.* **373**, 20170012 (2018).
3. M. P. Veldhuis *et al.*, Cross-boundary human impacts compromise the Serengeti–Mara ecosystem. *Science (1979)* **363**, 1424–1428 (2019).
4. M. Gong *et al.*, Wildebeest-derived malignant catarrhal fever: A bovine peripheral T cell lymphoma caused by cross-species transmission of *Alcelaphine gammaherpesvirus 1*. *Viruses* **15**, 526 (2023).
5. W. Plowright, R. D. Ferris, G. R. Scott, Blue wildebeest and the aetiological agent of bovine malignant catarrhal fever. *Nature* **188**, 1167–1169 (1960).
6. W. Plowright, Malignant catharrhal fever in East Africa. 1. Behaviour of the virus in free living populations of blue wildebeest (*Gorgon taurinus taurinus*, Burchell). *Res. Vet. Sci.* **6**, 56–68 (1965).
7. W. Plowright, Malignant catarrhal fever, in East Africa. II. Observations on wildebeest calves at the laboratory and contact transmission of the infection to cattle. *Res. Vet. Sci.* **6**, 69–83 (1965).
8. W. Plowright, Malignant catarrhal fever in East Africa 3. Neutralizing antibody in free-living wildebeest. *Res. Vet. Sci.* **8**, 129–136 (1967).
9. C. Bedelian, D. Nkedianye, M. Herrero, Maasai perception of the impact and incidence of malignant catarrhal fever (MCF) in southern Kenya. *Prev. Vet. Med.* **78**, 296–316 (2007).
10. D. Nthiwa, S. Alonso, D. Odongo, E. Kenya, B. Bett, A participatory epidemiological study of major cattle diseases amongst Maasai pastoralists living in wildlife-livestock interfaces in Maasai Mara, Kenya. *Trop. Anim. Health Prod.* **51**, 1097–1103 (2019).
11. D. Mlilo *et al.*, The epidemiology of malignant catarrhal fever (MCF) and contribution to cattle losses in farms around Rhodes Matopos National Park, Zimbabwe. *Trop. Anim. Health Prod.* **47**, 989–994 (2015).
12. F. Lankester *et al.*, The economic impact of malignant catarrhal fever on pastoralist livelihoods. *PLoS ONE* **10**, e0116059 (2015).
13. W. Plowright, "Chapter 14: Malignant catarrhal fever virus" in *Virus Infections of Ruminants, Virus Infections of Vertebrates Series*, Z. Dinter, B. Morein, Eds. (Elsevier, 1990), pp. 123–150.
14. B. G. B. G. Dewals, A. Vanderplasschen, Malignant catarrhal fever induced by *Alcelaphine herpesvirus 1* is characterized by an expansion of activated CD3+CD8+CD4- T cells expressing a cytotoxic phenotype in both lymphoid and non-lymphoid tissues. *Vet. Res.* **42**, 95 (2011).
15. B. Dewals *et al.*, Ex vivo bioluminescence detection of *Alcelaphine herpesvirus 1* infection during malignant catarrhal fever. *J. Virol.* **85**, 6941–6954 (2011).
16. B. Dewals, C. Boudry, F. Farnir, P.-V. Drion, A. Vanderplasschen, Malignant catarrhal fever induced by *Alcelaphine herpesvirus 1* is associated with proliferation of DC8+ T cells supporting a latent infection. *PLoS ONE* **3**, e1627 (2008).
17. B. Dewals *et al.*, Cloning of the genome of *Alcelaphine herpesvirus 1* as an infectious and pathogenic bacterial artificial chromosome. *J. Gen. Virol.* **87**, 509–517 (2006).

18. O. Sorel *et al.*, Small RNA deep sequencing identifies viral microRNAs during malignant catarrhal fever induced by *Alcelaphine herpesvirus 1*. *J. Gen. Virol.* **96**, 3360–3372 (2015).
19. L. Palmeira *et al.*, An essential role for gamma-herpesvirus latency-associated nuclear antigen homolog in an acute lymphoproliferative disease of cattle. *Proc. Natl. Acad. Sci. U.S.A.* **110**, E1933-42 (2013).
20. A. Schock, H. W. Reid, Characterisation of the lymphoproliferation in rabbits experimentally affected with malignant catarrhal fever. *Vet. Microbiol.* **53**, 111–119 (1996).
21. D. P. Dittmer, B. Damania, S. H. Sin, Animal models of tumorigenic herpesviruses–An update. *Curr. Opin. Virol.* **14**, 145–150 (2015).
22. B. Damania, Oncogenic gamma-herpesviruses: Comparison of viral proteins involved in tumorigenesis. *Nat. Rev. Microbiol.* **2**, 656–668 (2004).
23. F. Myster *et al.*, Genomic duplication and translocation of reactivation transactivator and bZIP-homolog genes is a conserved event in *Alcelaphine herpesvirus 1*. *Sci. Rep.* **6**, 38607 (2016).
24. O. Sorel *et al.*, Macavirus latency-associated protein evades immune detection through regulation of protein synthesis in cis depending upon its glycin/glutamate-rich domain. *PLoS Pathog.* **13**, e1006691 (2017).
25. C. Boudry *et al.*, The A5 gene of *Alcelaphine herpesvirus 1* encodes a constitutively active G-protein-coupled receptor that is non-essential for the induction of malignant catarrhal fever in rabbits. *J. Gen. Virol.* **88**, 3224–3233 (2007).
26. F. Myster *et al.*, *Alcelaphine herpesvirus 1* genes A7 and A8 regulate viral spread and are essential for malignant catarrhal fever. *PLoS Pathog.* **16**, 1–26 (2020).
27. N. Parameswaran *et al.*, The A2 gene of *Alcelaphine herpesvirus-1* is a transcriptional regulator affecting cytotoxicity in virus-infected T cells but is not required for malignant catarrhal fever induction in rabbits. *Virus Res.* **188**, 68–80 (2014).
28. F. Myster *et al.*, Viral semaphorin inhibits dendritic cell phagocytosis and migration but is not essential for gammaherpesvirus-induced lymphoproliferation in malignant catarrhal fever. *J. Virol.* **89**, 3630–3647 (2015).
29. M. Gong *et al.*, Deep sequencing after alcelaphine gammaherpesvirus 1 infection reveals the nature of CD8+ T cell expansion and identify an essential viral protein for fatal bovine malignant catarrhal fever. Gene Expression Omnibus (GEO). https://www.ncbi.nlm.nih.gov/geo/query/acc.cgi?acc=GSE253729. Deposited 19 January 2024.
30. S. J. Carmona, I. Siddiqui, M. Bilous, W. Held, D. Gfeller, Deciphering the transcriptomic landscape of tumor-infiltrating CD8 lymphocytes in B16 melanoma tumors with single-cell RNA-Seq. *Oncoimmunology* **9**, 1737369 (2020).
31. M. Rodríguez *et al.*, Peripheral T-cell lymphoma: Molecular profiling recognizes subclasses and identifies prognostic markers. *Blood Adv.* **5**, 5588–5598 (2021).
32. P. Naluyima *et al.*, Terminal effector CD8 T cells defined by an IKZF2+IL-7R− transcriptional signature express FcγRIIIA, expand in HIV infection, and mediate potent HIV-specific antibody-dependent cellular cytotoxicity. *J. Immunol.* **203**, 2210–2221 (2019).
33. P. Bost *et al.*, Host-viral infection maps reveal signatures of severe COVID-19 patients. *Cell* **181**, 1475–1488.e12 (2020).
34. H. Fickenscher, B. Fleckenstein, *Herpesvirus saimiri*. *Philos. Trans. R. Soc. Lond. B, Biol. Sci.* **356**, 545–567 (2001).
35. N.-H. Cho *et al.*, Inhibition of T cell receptor signal transduction by tyrosine kinase–interacting protein of *Herpesvirus saimiri*. *J. Exp. Med.* **200**, 681–687 (2004).
36. O. Khan *et al.*, TOX transcriptionally and epigenetically programs CD8+ T cell exhaustion. *Nature* **571**, 211–218 (2019).
37. A. C. Scott *et al.*, TOX is a critical regulator of tumour-specific T cell differentiation. *Nature* **571**, 270–274 (2019).
38. F. Alfei *et al.*, TOX reinforces the phenotype and longevity of exhausted T cells in chronic viral infection. *Nature* **571**, 265–269 (2019).
39. C. Yao *et al.*, Single-cell RNA-seq reveals TOX as a key regulator of CD8+ T cell persistence in chronic infection. *Nat. Immunol.* **20**, 890–901 (2019).
40. H. Seo *et al.*, TOX and TOX2 transcription factors cooperate with NR4A transcription factors to impose CD8+ T cell exhaustion. *Proc. Natl. Acad. Sci. U.S.A.* **116**, 12410–12415 (2019).
41. Q. P. Vong *et al.*, TOX2 regulates human natural killer cell development by controlling T-BET expression. *Blood* **124**, 3905–3913 (2014).
42. W. Xu *et al.*, The transcription factor Tox2 drives T follicular helper cell development via regulating chromatin accessibility article the transcription factor Tox2 drives T follicular helper cell development via regulating chromatin accessibility. *Immunity* **53**, 1–14 (2019).
43. M. Altmann, W. Hammerschmidt, Epstein-Barr virus provides a new paradigm: A requirement for the immediate inhibition of apoptosis. *PLoS Biol.* **3**, e404 (2005).
44. F. Lankester *et al.*, *Alcelaphine herpesvirus-1* (malignant catarrhal fever virus) in wildebeest placenta: Genetic variation of ORF50 and A9.5 alleles. *PLoS ONE* **10**, e0124121 (2015).
45. G. C. Russell *et al.*, A novel spliced gene in *Alcelaphine herpesvirus 1* encodes a glycoprotein which is secreted in vitro. *J. Gen. Virol.* **94**, 2515–2523 (2013).
46. S. M. Duboise, J. Guo, S. Czajak, R. C. Desrosiers, J. U. Jung, STP and tip are essential for *Herpesvirus saimiri* oncogenicity. *J. Virol.* 72, 1308–1313 (1998).
47. J. Hart *et al.*, Complete sequence and analysis of the ovine herpesvirus 2 genome. *J. Gen. Virol.* **88**, 28–39 (2007).
48. N. S. Taus *et al.*, Comparison of ovine herpesvirus 2 genomes isolated from domestic sheep (*Ovis aries*) and a clinically affected cow (*Bos bovis*). *J. Gen. Virol.* **88**, 40–45 (2007).
49. S. M. Duboise *et al.*, Mutation of the Lck-binding motif of tip enhances lymphoid cell activation by *Herpesvirus saimiri*. *J. Virol.* 72, 2607–2614 (1998).
50. J. Park *et al.*, Herpesviral protein targets a cellular WD repeat endosomal protein to downregulate T lymphocyte receptor expression. *Immunity* **17**, 221–233 (2002).